IGSHPA Research Track
Las Vegas, December 6-8, 2022

A Case Study on High-Resolution Monitoring Network of Groundwater Heat Pump System

Ji-Young Baek **Hae-Rim Oh** **Seung-Wook Ha**
Seong-Sun Lee **Kang-Kun Lee**

ABSTRACT

With the increasing installation of shallow geothermal energy, the importance of thermal impact prediction also increases in the system design stage. In nature, it is general that heterogeneity exists and it can affect the groundwater flow as well as the transport along to the flow. When predicting heat transport under the groundwater heat pump (GWHP) operation, however, impacts of heterogeneity have rarely been considered. In this study, to detect the hydraulic and thermal feedback to the two months of GWHP operation, a dense monitoring network was constructed with 12 monitoring wells at Eumseong-gun, Republic of Korea. The temperature was monitored in high resolution via fiber-optic distributed temperature sensing. During the GWHP operation, a very dynamic flow condition was generated with the hydraulic gradient between 0.005 and 0.07. The maximum temperature change at the nearest monitoring well was 2 ℃. Observed hydraulic and thermal responses showed spatially heterogeneous results. While the heterogeneous responses of hydraulic change were stronger near the geothermal wells, those of temperature change were higher near the center of the thermal plume.

INTRODUCTION

In general, since nature is not homogeneous, the aquifer properties are shown spatial variability that can affect both groundwater flow and transport (Wu et al., 2005). The impacts of hydraulic heterogeneity on groundwater flow have been investigated by the systematic hydraulic tests in laboratory and field scales, or by the numerical model (Schwede et al., 2014; Somogyvari et al., 2017). The heterogeneity of aquifer also can affect heat transport occurring along with the groundwater flow and its impacts on transport results were studied through the tracer experiments and numerical model (Hamidi et al., 2019; Hoffmann et al., 2019). As several studies highlighted, the local heterogeneity can significantly affect hydraulic conditions near the injection and extraction points. Especially, under the GWHP operation, more complex flow is generated due to the dynamic injection environment. Although those complex flows can affect the flow and heat transport, the dense monitoring to consider the impacts of heterogeneity on thermal plume propagation during the dynamic injection environment has rarely been constructed and interpreted for the real scale experiments.

In this study, the GWHP system was installed at Eumseong-gun, Republic of Korea, and dense monitoring network was constructed with 12 monitoring wells. Especially, for temperature monitoring, fiber optic distributed temperature sensing was applied to obtain high-resolution spatial temperature data. Through the monitoring network, the hydraulic and thermal responses to the operation of the GWHP system were observed. Based on the observed temperature time-series data, the thermal front velocities were estimated for different four depths to figure out the impacts of inherent heterogeneity on flow and heat transport.

Kang-Kun Lee (kklee@snu.ac.kr) is a professor of school of earth and environmental sciences and Ji-Young Baek, Hae-Rim Oh, Seung-Wook Ha are PhD students and Seong-Sun Lee is a senior researcher at Seoul National University.

DOI: https://doi.org/10.22488/okstate.22.000025

METHODS AND MATERIALS

Site description

The study area is located in Eumseong-gun, Republic of Korea. According to the watershed divides, it is contained in the Upper Miho Stream watershed, the north-center of the Geum River watershed. The geological composition of the study site is mainly explained by Jurassic Daebo granites (Kee et al., 2020). The sample core data of the borehole and the seismic refraction survey results showed the weathered soil covered a weathered rock layer which appears about 43 m in depth. The weathered rock consists of weathered biotite granite, and the main mineral composition of highly weathered biotite granite is quartz, albite, anorthite, and microcline with a small amount of hornblende, illite, and chlorite (Ju et al., 2022).

Two geothermal wells and 12 monitoring wells were fully screened for 40 m in depth. The ET of 76 m in depth consists of a polyethylene pipe and grouting material (bentonite for this site) to conduct the thermal response test. A background groundwater flow was locally generated from east to west in this site with a hydraulic gradient of 0.006 ± 0.0004. The overall water level distribution was in the range of 76.24 m (a.s.l) and 76.40 m (a.s.l.). For background groundwater temperatures within a site, there were few temperature differences in a horizontal direction with a small standard deviation of 0.05 ℃, lower than the sensor accuracy (Figure 1). The mean background groundwater temperature on all monitoring wells was 13.7 ℃. The hydraulic conductivity was determined as 1.97–2.98 m/d, using AQTESOLV (HydroSOLVE, Inc., USA) software to analyze the pumping test carried out at EM6 for 10.7 h by 16.6 m^3/d.

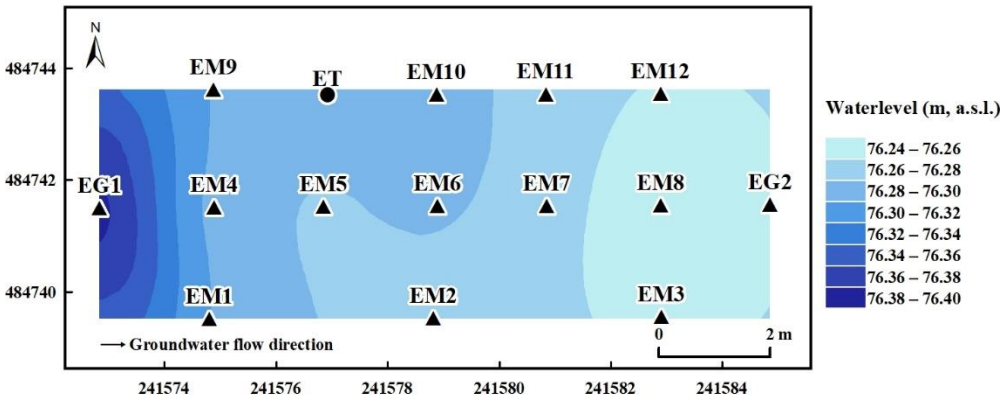

Figure 1 Background hydraulic head distribution. The ET is the borehole heat exchanger to conduct the thermal response test, EG wells are geothermal wells, and EM wells are monitoring wells.

GWHP system operation and monitoring network

A groundwater heat pump (GWHP) system was installed at the study site with two geothermal wells (EG1 and EG2 in Figure 1) and a monitoring network was densely constructed with 12 monitoring wells (EM1–12 in Figure 1) to catch the environmental change within groundwater able to reflect inherent local heterogeneity. To extract groundwater for heat exchange, a 1 HP submersible pump (ST-1808, Stairspumps, Republic of Korea) was installed at the 30 m depth of EG2 (pumping well). The pump was connected to the circulation pipeline which enable an indirect exchange of its

heat through the heat exchanger (Daesungheatenersys, Republic of Korea). Groundwater that temperature had been changed after the heat exchange was re-injected into EG1 (injection well). The GWHP system operated in a cooling mode from June 2, 2021, to July 31, 2021 (58 days).

For the real-time recording of the system operation status, a developed software was used to automatically control the GWHP system by regulating the power supply to the heat exchanger. The software recorded the operation state, load and source temperatures, and flow rate in the one-minute interval. Environmental changes due to the GWHP system were monitored by data loggers in terms of water level, temperature, and EC. TD-Diver (Schlumberger, The Netherlands) was selected to detect the water level as well as temperature and was installed at the 20 m depth of all monitoring wells. For the groundwater temperature and EC monitoring, CTD-Diver (Schlumberger, The Netherlands), and Levelogger LTC (Solinst, Canada) were installed at the 30 m depth of all monitoring wells. For the hydraulic head data, water level changes logged by TD-Diver were corrected via barometric pressure changes detected by Barologger (Solinst, Canada) installed at the 15 m depth of EM6. All loggers recorded the data in ten-minute intervals during and after the operation. In addition, a fiber-optic distributed temperature sensing (FO-DTS) system (Woori-system, Republic of Korea) was employed for temperature monitoring to obtain the temperature profile of each well. A 1600 m long two-core FO cable (SUS ARMORED, Woori-system, Republic of Korea) was installed at entire wells except for EG2 and it was connected to a DTS device (DTSX3000, Yokogawa, Japan) to detect the temperature changes. The applied FO-DTS system measured the temperature in less than one-second intervals with an accuracy of 0.5 ℃ and a spatial resolution of 1 m. For the temperature data measured by FO-DTS, pre-processing was performed by moving averaging to reduce the data noise. Detailed information on the constructed monitoring network is organized in Table 1.

Table 1. Detailed information on the monitoring system

Device (Manufacturer)	Installed well ID	Installed depth (m, b.g.s.)	Interval	Monitoring factors	Accuracy
TD-Diver (Schlumberger)	EG1, EM1–12	20 m	10 min	Water level Temperature	1 cmH_2O 0.1 ℃
CTD-Diver (Schlumberger)	EM1–3, 8–10, 12	30 m	10 min	Water level Temperature EC	2.5 cmH_2O 0.1 ℃ 1 % of reading
Levelogger LTC (Solinst)	EM4–7	30 m	10 min	Water level Temperature EC	5 cmH_2O 0.05 ℃ 0.1 μS/cm
FO-DTS (Woori-system)	EM1–12, EG1	Spatial resolution: 1 m	< 1 s	Temperature	0.5 ℃

Thermal front velocity estimation

According to Levec and Carbonell (1985), when the thermal velocity in the fluid is the same as in the solid, the thermal front velocity can be expressed by the seepage velocity and volumetric heat capacity ratio as follows:

$$v^t = v^s/R \tag{1}$$

where the R is defined by (Bodvarsson, 1972)

$$R = \rho c/n_e \rho_f c_f \tag{2}$$

The seepage velocity can be written using Darcy's law as (Fetter, 2001)

$$v^s = q/n_e = Ki/n_e \tag{3}$$

With Eqs. (2) and (3), Eq. (1) can be rewritten as

$$v^t = v^s/R = Ki\rho_f c_f/\rho c \quad (4)$$

Thermal front velocity can be additionally estimated by the cross-correlation analysis of obtained temperature time-series. For time-series x_t and y_t, the cross-correlation coefficient at d is given by (Lo Russo et al., 2018)

$$r_{xy}(d) = C_{xy}(d)/\sigma_x\sigma_y \quad (5)$$

where

$$C_{xy}(d) = \frac{1}{N}\sum_{t=1}^{N-d}(x_t - \bar{x})(y_{t+d} - \bar{y}) \quad (6)$$

Thermal front velocity calculated by temperature time-series is defined as (Lo Russo et al., 2018)

$$v^t = D/L \quad (7)$$

where D [d] is the lag at the maximum r_{xy}.

RESULTS

Environmental changes during GWHP system operation

Water level change during the GWHP system operation. In the GWHP system, the injection and extraction occur repeatedly, but irregularly according to the heating or cooling demands. Due to that characteristic, complex hydraulic conditions can be generated during the operation. In this study, we monitored the environmental changes to investigate the flow and heat transport during the GWHP system considering the complex hydraulic conditions. The water level was monitored at 12 monitoring wells and the injection well at time intervals of ten minutes. In the results, while the background hydraulic gradient from EM4 to EM8 was relatively constant at 0.006 on average, during the GWHP operation, it showed a dynamic change up to 0.2 following the operation state.

Fig. 2 shows the observed hydraulic head data which was corrected by barometric pressure changes and elevation. In this study, the data were spatially divided into three parts: near the injection well (EM1, EM4, and EM9), the middle part (EM2, EM6, and EM10), and near the extraction well (EM3, EM8, and EM12). Near the injection well and the extraction well, the observed water levels showed a dynamic variation along with the complex cycle of system operation. The hydraulic head changes due to the injection and extraction were similar at monitoring wells that had the same distance to the injection and extraction wells. For example, water level changes at EM4 (2 m from the injection well) and EM8 (2 m from the extraction well) were 0.71 m and 0.75 m. However, the change patterns were different for the injection and extraction (Fig. 2a and Fig. 2c). In the middle part, where the distance to the injection well or the extraction well was the same (EM2, EM6, and EM10), the hydraulic head change was not noticeable due to the superposition effect of injection and extraction (Fig. 2b). Comparing the upper and lower parts, the hydraulic head change showed a spatial difference as it was larger in the upper part (EM9, and EM12) than in the lower part (EM1, and EM3) except for the EM2, and EM10.

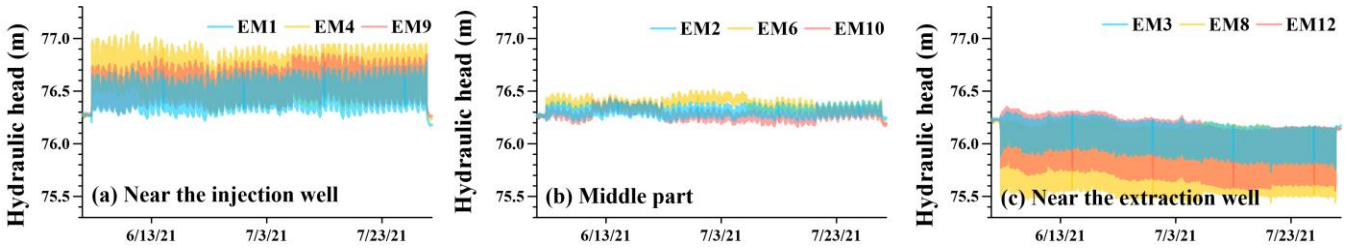

Figure 2 Observed hydraulic head at monitoring wells during the operation of the GWHP system (a) near the injection well, (b) at the middle part, and (c) near the extraction well.

Groundwater temperature changes during the GWHP system operation. During the GWHP system, the temperature change was monitored at the depth of 20 and 30 m by the temperature loggers as explained in Table 1. Also, in this study, we applied the FO-DTS method, which can record the temperature every 1 m depth at 12 monitoring wells and the injection well in real time, to obtain high-resolution temperature data in terms of spatial distribution. It was anticipated that the high-resolution data would enable an investigation of the impacts of heterogeneity on thermal plume propagation both in horizontal and vertical directions. The two temperature data, measured by temperature loggers and FO cable, showed good agreement with the averaged RMSE of 0.1 ℃ which is not exceeding the accuracy of the FO-DTS (0.5 ℃) and temperature logger (0.1 ℃). Especially for the wells that showed a temperature change of more than 0.9 ℃ (EM1–2, EM4–6, EM9–10, and EG1), the R-squared value was larger than 0.943. These results could ensure the applicability of FO-DTS in the detection of groundwater temperature changes during the GWHP system operation.

Figure 3 showed the spatial difference between the measured temperatures at the depths of 20 m and 30 m. The difference between the two temperature data was in the range of -0.2 ℃ to 0.8 ℃ and it increased along with the plume migration. The temperature difference between the two depths showed temporal and spatial variance, which can be evidence of the heterogeneity. For example, if the ground was homogeneous since injected hot water was transported along the groundwater flow direction, the temperature difference at the monitoring well cannot exceed that at the injection well. However, the experimental results showed that the maximum temperature difference at EM5 (monitoring well) was larger than that at EG1 (injection well). In other words, the thermal plume propagated faster at 20 m depth compared to at 30 m depth.

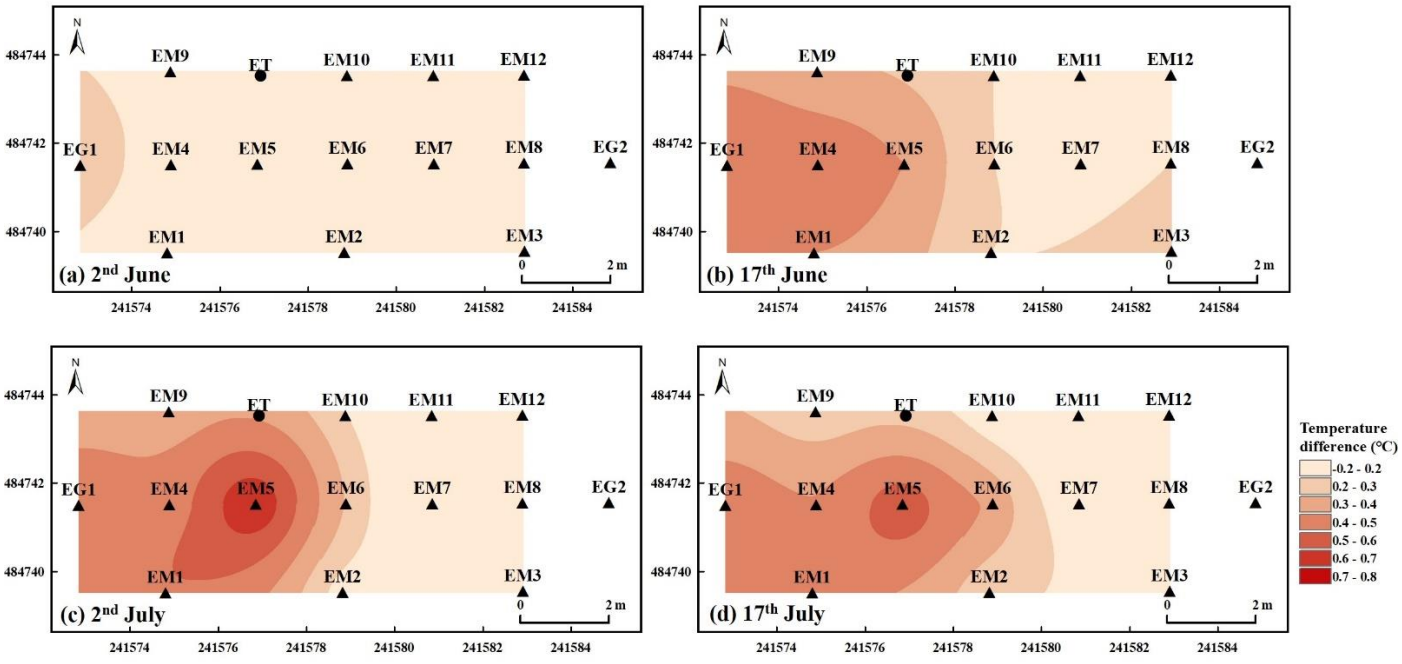

Figure 3 Spatial distribution of temperature difference between the depths of 20 m and 30m.

Estimated thermal front velocity

In this study, thermal front velocities were estimated by two different methods. That is the *theoretical* v^t (Eq. 4), calculated by the physical properties of the aquifer, and the *experimental* v^t (Eq. 7), estimated by the time delay of temperature time-series between two different wells. The *theoretical* v^t was calculated using the maximum and minimum values of hydraulic gradients and hydraulic conductivity. In this study, calculated *theoretical* v^t ranged from 0.10 m/d to 0.72 m/d (Fig. 4).

For the analysis of *experimental* v^t, the monitoring wells along the groundwater flow equations were used (EM1–EM2, EM4–EM7, and EM9–EM11) except EM3, EM8, and EM12 where the maximum temperature difference was lower than the sensing accuracy of FO-DTS (0.5 ℃). The analysis was carried out using temperature data obtained from FO–DTS at four different depths of 20 m, 25 m, 30 m, and 35 m. In the cross-correlation analysis, the maximum cross-correlation coefficient of each case was larger than 0.62. The maximum cross-correlation coefficients were decreased with the increase of the well distance, which can indicate the correlation between the two time-series data was diminished according to the propagation of the thermal plume. In four cases, however, the cross-correlation was the highest from the very first time so the determined lag was minimal (e.g., d = 1 min) that was not reliable for representing the thermal velocity between the wells. Except for four cases, the resulted *experimental* v^t was in the range of 0.32 m/d to 1.21 m/d which was in a comparable range to the theoretical v^t (Fig. 4). Based on these results, it could be confirmed that the *experimental* v^t was reasonably estimated.

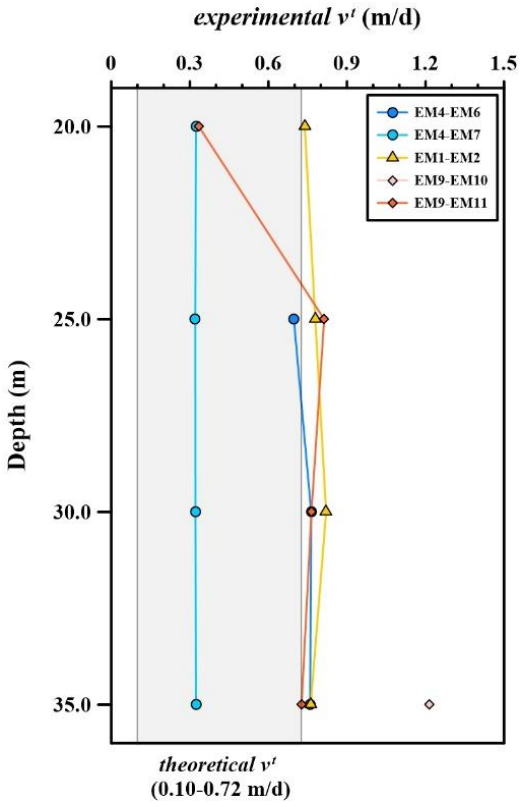

Figure 4 Calculated *theoretical* v^t for the study area and *experimental* v^t estimated at the specific depths (20, 25, 30, and 35 m).

CONCLUSION

In this study, the hydraulic and thermal changes were observed by a densely constructed monitoring network during the operation of the GWHP system installed in Eumseong-gun, Republic of Korea. To obtain high-resolution spatial temperature data, fiber optic distributed temperature sensing was applied. In the results, depth-averaged hydraulic responses to the GWHP system operation were different in monitoring wells that have the same distance to the geothermal wells, and those heterogeneous responses appeared stronger near the injection and extraction wells. Heterogeneity of thermal response appeared both vertical and horizontal. The vertical difference was the highest where the center of the thermal plume migrated. The estimated thermal front velocity supported the temperature monitoring results as it was different not only to the well intervals but also to the depths. As a further analysis, an inverse modeling will be performed using a numerical simulation to figure out the spatial distribution of effective hydraulic parameters. Based on that result, heat transport reflecting the hydraulic heterogeneity will be modeled to find out the possible impacts of heterogeneity on thermal plume propagation a short and long period of GWHP system operation.

ACKNOWLEDGMENTS

This work was supported by the National Research Foundation of Korea (NRF) grant funded by the Korea government (MSIP) (No. 2022R1A2C1006696).

NOMENCLATURE

v^t = Thermal front velocity (m/d)
v^s = Seepage velocity (m/d)
R = Retardation factor (-)
n_e = Effective porosity (-)
ρc = Volumetric heat capacity (J/m^3/K)
q = Specific discharge (m/d)
K = Hydraulic conductivity (m/d)
i = Hydraulic gradient (-)
d = Lag (d)
N = Length of data (-)
σ = Standard deviation of the time series (°C)
L = Distance between two points (m)

Subscripts

f = fluid

REFERENCES

Bodvarsson, G. 1972. *Thermal problems in the siting of reinjection wells*. Geothermics 1(2): 63-66.

Fetter, C.W. 2001. *Applied Hydrogeology*. Upper Saddle River, NJ: Prentice-Hall Inc.

Hamidi, S., Heinze, T., Galvan, B., and Miller, S. 2019. *Critical review of the local thermal equilibrium assumption in heterogeneous porous media: Dependence on permeability and porosity contrasts*. Applied Thermal Engineering 147: 962-971.

Hoffmann, R., Dassargues, A., Goderniaux, P., and Hermans, T. 2019. *Heterogeneity and prior uncertainty investigation using a joint heat and solute tracer experiment in alluvial sediments*. Frontiers in Earth Science 7, 108.

Kee, W. S., Kim, S. W., Hong, P. S., Lee, B. C., Cho, D. R., Byun, U. H., ... and Lee, H. J. 2020. *1: 1,000,000 Geological map of Korea*. Korea Institute of Geoscience and Mineral Resources.

Ju, Y., Györe, D., Gilfillan, S. M., Lee, S. S., Cho, I., Ha, S. W., ... and Lee, K. K. 2022. *Constraining the effectiveness of inherent tracers of captured CO2 for tracing CO2 leakage: Demonstration in a controlled release site*. Science of the Total Environment, 824, 153835.

Levec, J. and Carbonell, R. G. 1985. *Longitudinal and lateral thermal dispersion in packed beds. Part I: Theory*. AIChE journal 31(4): 581-590.

Lo Russo, S., Taddia, G., Dabove, P., Cerino Abdin, E., and Manzino, A. M. 2018. *Effectiveness of time-series analysis for thermal plume propagation assessment in an open-loop groundwater heat pump plant*. Environmental Earth Sciences 77(18): 1-11.

Schwede, R. L., Li, W., Leven, C., and Cirpka, O. A. 2014. *Three-dimensional geostatistical inversion of synthetic tomographic pumping and heat-tracer tests in a nested-cell setup*. Advances in water resources 63: 77-90.

Somogyvári, M. and Bayer, P. 2017. *Field validation of thermal tracer tomography for reconstruction of aquifer heterogeneity*. Water Resources Research 53(6): 5070-5084.

Wu, J., Hu, B. X., and He, C. 2004. *A numerical method of moments for solute transport in a porous medium with multiscale physical and chemical heterogeneity*. Water resources research 40(1).